Available online at www.sciencedirect.com
SCIENCE DIRECT®
Journal of Nuclear Materials 327 (2004) 121–129
journal of nuclear materials
www.elsevier.com/locate/jnucmat

Microstructure of U_3Si_2 fuel plates submitted to a high heat flux

A. Leenaers [a,*], S. Van den Berghe [a], E. Koonen [a], P. Jacquet [a], C. Jarousse [b], B. Guigon [c], A. Ballagny [c], L. Sannen [a]

[a] SCK•CEN, Reactor Materials Research, Boeretang 200, B-2400 Mol, Belgium
[b] CERCA, ZI Les Bérauds, 26104 Romans, France
[c] Commissariat à l'énergie atomique (CEA), Centre de Cadarache, 13108 Saint Paul lez Durance cedex, France

Received 2 December 2003; accepted 27 January 2004

Abstract

In order to gain insight on the performance limits of U_3Si_2 fuel with Al cladding, fuel plates with a fissile material density of 5.1 and 6.1 g U/cm^3 were irradiated in the BR2 reactor of SCK•CEN in Mol. The plates were intended to be subjected to severe conditions leading to a cladding surface temperature of 180–200 °C and fuel temperatures of 220–240 °C. The irradiation program was stopped after the second cycle based on the visual inspection and wet sipping tests of the elements, correspondingly showing degradations on the outer Al surfaces of the U_3Si_2 plates and the release of fission products. The maximum fuel burn-up was 29% and 25% ^{235}U, respectively. In a PIE program the microstructural causes for this degradation are analysed. It is found that the failure of the plates is entirely related to the corrosion of the Al cladding, which has caused temperatures to rise well beyond the calculated values. In all stages, the fuel grains have retained their integrity and, apart from the formation of an interaction phase with the Al matrix, they do not demonstrate deleterious changes in their physical properties.

1. Introduction

The design of the French Réacteur Jules Horowitz (RJH) is based on low enriched uranium (LEU) fuel ($\leqslant 20\%$ $^{235}U/U_{total}$). In LEU fuel the reduction of the enrichment or fissile material is compensated by a higher uranium loading density [1,2]. As manager of the RJH project, the Commissariat à l' énergie atomique (CEA) has a vital interest in the qualification of LEU fuels. Such a program requires irradiation tests to demonstrate the ability of the fuel to withstand research reactor operating limits (i.e. high power densities) up to economically viable burn-up values. Among the fuels considered is the U_3Si_2 fuel dispersed in an aluminum matrix [3]. U_3Si_2 has been found to perform well under irradiation tests, even with uranium densities up to 5.0 g/cm^3 [4].

To study the performance limits of this fuel type, U_3Si_2 fuel plates have been irradiated in the BR2 reactor of SCK•CEN in Mol. The objective of the irradiation program was to test the behavior of the U_3Si_2 plates under conditions corresponding to the upper boundary limit of the regime at which the RJH reactor is planned to operate. As such, the plates have been submitted to a high local heat flux, resulting in elevated cladding and fuel temperatures. After irradiation, visual inspection of the fuel elements showed important degradations of the outer surfaces of the U_3Si_2 plates, including visible swelling. Wet sipping tests demonstrated loss of integrity for one of the fuel plates.

Several samples have been cut from the fuel plates and investigated in a post-irradiation program by optical microscopy (OM), scanning electron microscopy (SEM) and electronprobe microanalysis (EPMA). In

* Corresponding author. Tel.: +32-14 333044; fax: +32-14 321216.
E-mail address: aleenaer@sckcen.be (A. Leenaers).

0022-3115/$ - see front matter © 2004 Elsevier B.V. All rights reserved.
doi:10.1016/j.jnucmat.2004.01.025

this article, the results of the microstructural examination of the fuel plate with the highest U loading (6.1 g U/cm^3) are presented. It should be noted at this point that although the fuel plates have a different uranium loadings (5.1 g U/cm^3 and 6.1 g U/cm^3), their behavior is similar and depends only on the heat flux and consequently the temperature, which they have generated.

2. Experimental

2.1. Fuel plates and irradiation history

A standard BR2 element (Fig. 1) consists of six concentric tubes, each tube being an assembly of three equal curved segments made of rolled plates which are mechanically fixed by the roll swaging technique into three solid grooved radial stiffeners. Six U_3Si_2 fuel plates manufactured by the Compagnie pour l'Etude et la Réalisation de Combustibles Atomiques (CERCA) in Romans (France) are used to constitute the outer cylinder of two standard BR2 elements. The two sets of U_3Si_2 fuel plates used, differ in uranium loading, i.e. 5.1 and 6.1 g U/cm^3.

The fissile material or meat consists of U_3Si_2 grains dispersed in a pure aluminum matrix with a mass ratio (U_3Si_2/Al) of, respectively, 4.2 and 6.6. The enrichment of the uranium amounts to 35% $^{235}U/U_{total}$. The cladding of the fuel elements is made of AG3-NET Al–Mg alloy (2.5–3 wt% Mg), which corresponds to a nuclear grade Al5754 alloy. One should bear in mind that, due to transmutation of Al by neutron capture, Si is formed and the alloy will evolve to an Al–Mg–Si alloy (6XXX series).

The fuel elements were incorporated in the BR2 reactor during two irradiation cycles. The reactor power was used for fine tuning the heat flux on the U_3Si_2 plates. Thermal hydraulic calculations performed with a finite element model showed that, if the BR2 reactor was operated at a power of 62.7 MW (110% of the nominal total reactor power), the requested mean heat flux in the axial hot plane would approach, but not exceed the requested 520 W/cm^2, which corresponds to the upper limit at which the RJH reactor is scheduled to operate. From the temperature calculations it was found that at that power, the external cladding surface temperature of the fuel plates would reach a value of around 160 °C. However, the azimuthal distribution of the heat flux in the axial hot plane of fuel element containing 6.1 g U/cm^3, shows in the first cycle a peak of 550 W/cm^2 close to the stiffener.

Fig. 1. Standard BR2 element consisting of six concentric tubes, each tube being an assembly of three equal curved segments (plates). In the described irradiation program six U_3Si_2 fuel plates constitute the outer cylinder of two standard BR2 elements.

During the second cycle, the power was reduced to 57 MW (100% of the nominal total reactor power), as DART code calculations predicted that all the aluminum of the fuel matrix would be consumed during this cycle, considering the burn-up in the U_3Si_2 fuel plates accumulated during the first cycle and the maximum temperatures associated with an operation at 62.7 MW. However, the second cycle was prematurely terminated.

After the partial second cycle, wet sipping tests showed the release of fission products by the element with the highest U loading. Visual inspection furthermore revealed important degradations of the outer surfaces and swelling of the U_3Si_2 plates of both elements. Based on this information, the irradiation program was stopped before the mean burn-up target of approximately 30% ^{235}U for the fuel element (i.e. ≈45% ^{235}U burn-up for the U_3Si_2 plate) had been reached and the U_3Si_2 fuel plates were recuperated. At their end-of-life the U_3Si_2 plates with a fissile material density of 5.1 g U/cm^3 and 6.1 g U/cm^3 showed a maximum burn-up of, respectively, 1.15×10^{21} and 1.29×10^{21} fissions/cm^3 (29 and 25% ^{235}U).

2.2. Post-irradiation examination

Visual examination at the reactor site hot cell revealed that the deformed zone on the fuel plates consists of 3 concentric half-circular stretched areas. The inner area, i.e. the area closest to the stiffener, shows a granite aspect, which would indicate pitting corrosion.

A special device has been designed and constructed to measure the thickness of the fuel plates. The plate is fixed in-between rotating clamps and two opposite linear variable differential transducer (LVDT) sensors are guided over the axis of the plate. The rotating clamps allow for axial scanning at different azimuthal positions permitting the complete plate surface to be measured. By calibrating the LVDT measuring device on a reference plate, a measurement accuracy for the plate thickness of ±5 μm is obtained. The result of the thickness measurement of the fuel plate with a density of 6.1 g U/cm^3 is presented in a 2-dimensional view in Fig. 2. The swelling

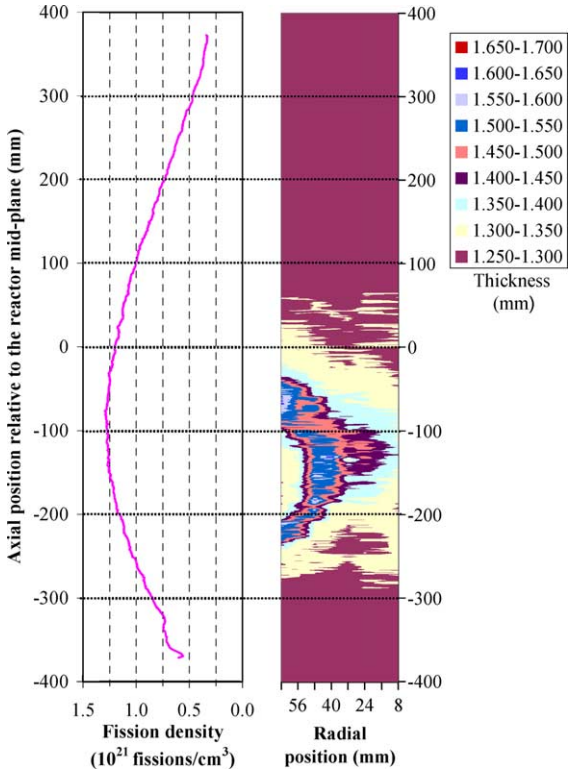

Fig. 2. The burn-up profile (left) and the thickness measurements (right) of the fuel plate show that the most deformed area coincides with an area of high burn-up and high heat flux, respectively, 1.29 fissions/cm^3 and 550 W/cm^2.

is located at the left side of the plate, at a position azimuthally located near the stiffener, where the fission density shows a maximum. Given the as-fabricated plate thickness (1.28 ± 0.01) mm, the swelling amounts up to about 0.33 mm.

Based on the profilometry of the fuel plates, several samples from each U_3Si_2 plate are cut from the fuel plates. The samples are embedded in an epoxy resin in such a way that the complete section of the fuel (meat and cladding) can be observed. The samples are polished with SiC paper of successively finer grain size, finishing on cloth with diamond paste of 3 and 1 μm. Optical microscopy is performed on a Reichert Telatom 3 remote-controlled and shielded optical microscope.

Before mounting in the electron microscope, the samples were coated with carbon to prevent charging. The electronprobe microanalysis (EPMA) is performed on a shielded CAMEBAX-R Microbeam, upgraded with digital image and X-ray acquisition programs (SAMx Suite). X-ray maps are recorded to obtain the lateral distribution of several elements (Al, Si, Mg, U, O, ...), and the elemental composition of the fuel plates is measured by wavelength dispersive X-ray analysis (WDX). Prior to each measurement, calibration is performed using the appropriate standards (Table 1). To convert the measured intensities to concentrations, a $\phi\rho z$ procedure is applied. A shielded JEOL scanning electron microscope type 6310 is used in backscattered electron image mode to detect fission gas bubbles in the fuel.

3. Results

3.1. Cladding corrosion

The low magnification ceramographic observation of the fuel section that has been submitted to a relatively low heat flux (approximately 450 W/cm^2), shows no visible degradation of the cladding or the fuel (Fig. 3(a)). The detailed image of the fuel (Fig. 3(b)) reveals an interaction phase (average thickness of 2 μm), between the U_3Si_2 particles (dark gray) and the aluminum matrix (white). Such an interaction layer is regularly observed for this type of fuel and has been identified as an $U(Al,Si)_3$ phase [5,6].

With increasing heat flux (approximately 500 W/cm^2) the oxidation of the cladding at the waterside surfaces becomes visible (Fig. 3(c)). A dense oxide layer has developed followed by a layer with a granular aspect

Table 1
Crystals used for X-ray map and quantitative EPMA analysis

Element	X-ray line	Wavelength (pm)	Crystal	Standard
O	Kα	2362.0	PC1	ZrO_2
Mg	Kα	989.5	TAP	Mg (pure)
Al	Kβ	794.0	TAP	Al_2O_3
Si	Kα	712.7	PET	Si (pure)
Mo	Lα	540.7	PET	Mo (pure)
Ru	Lα	484.7	PET	Ru (pure)
Xe	Lα	301.7	PET	Interpolation
Nd	Lα	237.1	LIF	NdF_3
U	Mα	391.0	PET	U (pure)
Pu	Mβ	371.6	PET	$(U,Pu)O_2$

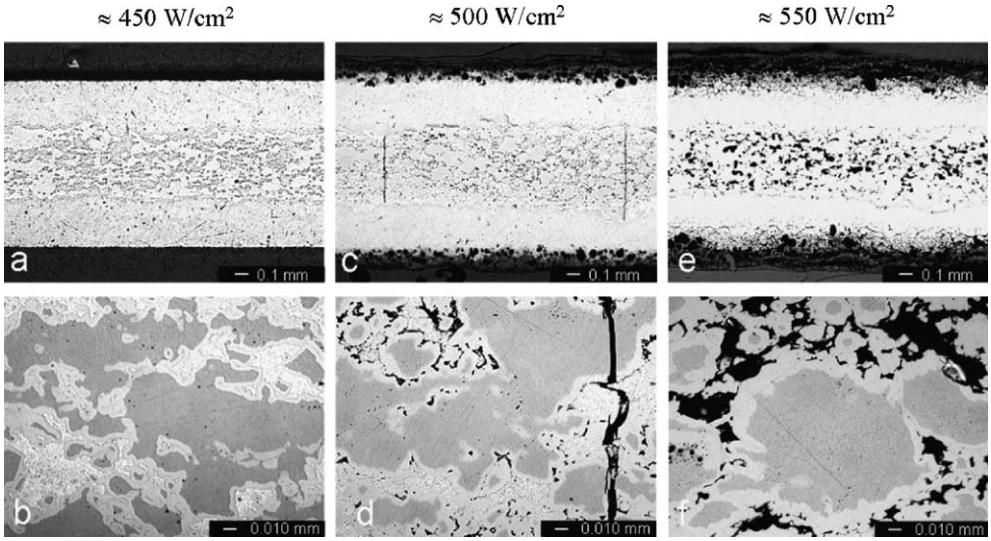

Fig. 3. Image of the fuel plate over the fuel width and a micrograph of the meat obtained from the section of the fuel plate that has been submitted to ≈450 W/cm² (a, b), ≈500 W/cm² (c, d) and ≈550 W/cm² (e, f).

which is most probably caused by pitting corrosion. In this section the fuel is relatively intact, with the exception of several larger cracks passing through the complete thickness of the meat (Fig. 3(d)). The origin of these cracks should be attributed to the thermal cycling of the fuel. The interaction between the U_3Si_2 particles and the aluminum matrix has progressed slightly further (average thickness of interaction layer equals 3 μm) but most of the particles are still separated by pure aluminum.

The image of the fuel plate section that has been submitted to 550 W/cm² (Fig. 3(e)) shows that the corrosion of the cladding has proceeded up to the meat. A clear increase in plate thickness of approximately 0.3 mm can be measured, which is in good agreement with the LVDT measurement (0.33 mm). As also visible in Figs. 3(a), (c) and (e), the swelling of the fuel plate should be attributed to the corrosion of the cladding and not to an increase of the meat thickness. In the meat, all the aluminum matrix is consumed by the fuel and large voids are present (Fig. 3(f)). The average thickness of the interaction layer has increased to 5 μm.

X-ray maps of the fuel plate sample submitted to 550 W/cm² are recorded to reveal the distribution of aluminum, magnesium, silicon and oxygen in the corroded cladding. From Fig. 4 it is clearly seen that the corroded cladding consists of several layers. A first layer (Fig. 4(L1)), with a thickness of approximately 100 μm, at the outer waterside surface of the cladding, is a dense oxide layer, without precipitates but containing some Mg. Below this layer, a pitting corrosion layer with characteristic corrosion pits can be seen (Fig. 4(L2)). Underneath, a network of grain boundaries is clearly delineated in the Mg and O X-ray maps (Fig. 4(L3)). It is also noticed that in this layer the grain interiors have been oxidised and contain oxidised Mg. In layer 4 (Fig. 4(L4)) only the grain boundaries have been affected and the grain interior shows clustering of Mg but as yet unoxidised. At this and the next position (Fig. 4(L5)), one can observe that Mg and Si particles are associated and form precipitates (Mg_2Si) in the cladding material.

Close to the meat (Fig. 4(L5)), a layer of relatively intact cladding is still present. At the interface between cladding and the meat, a layer of oxidised Mg (MgO) is observed (Fig. 4(L6)).

3.2. Fuel behavior

The U, Al and Si X-ray maps in the meat of the sample that has been submitted to a heat flux of 550 W/cm² (Fig. 5), indicate that the consumption of the aluminum matrix is complete and that a U–Si–Al interaction phase is present. Voids have formed between the fuel grains and the oxygen map shows the oxidation of the inner surfaces of these porosities. This indicates that water has intruded in the fuel causing the oxidation of the surface of the voids.

In the secondary electron image (Fig. 6(a)) of a U_3Si_2 fuel particle (1) at the Al cladding (2), the U–Si–Al interaction layer (3) is clearly outlined. In between the fuel particles pores have formed (4), again indicating complete consumption of the Al matrix. In the U_3Si_2 fuel particle, small bubbles can be observed. In the backscattered electron image of the same area (Fig. 6(b)), also the subsurface fission gas bubbles become visible.

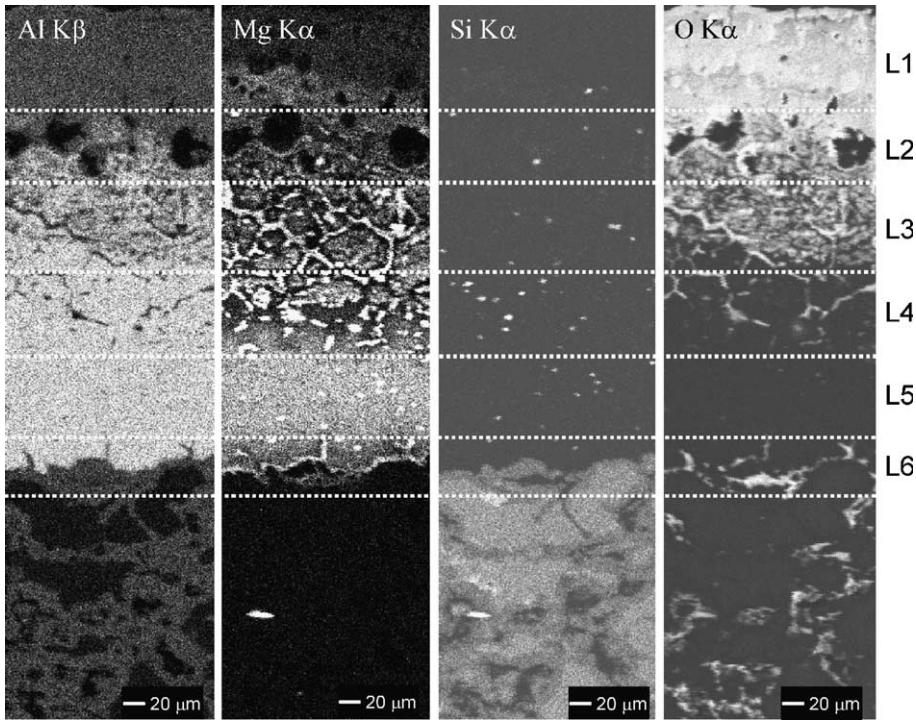

Fig. 4. AlKβ, MgKα, SiKα and OKα X-ray maps of the corroded cladding, allow to describe the corrosion process in different layers (L1 to L2).

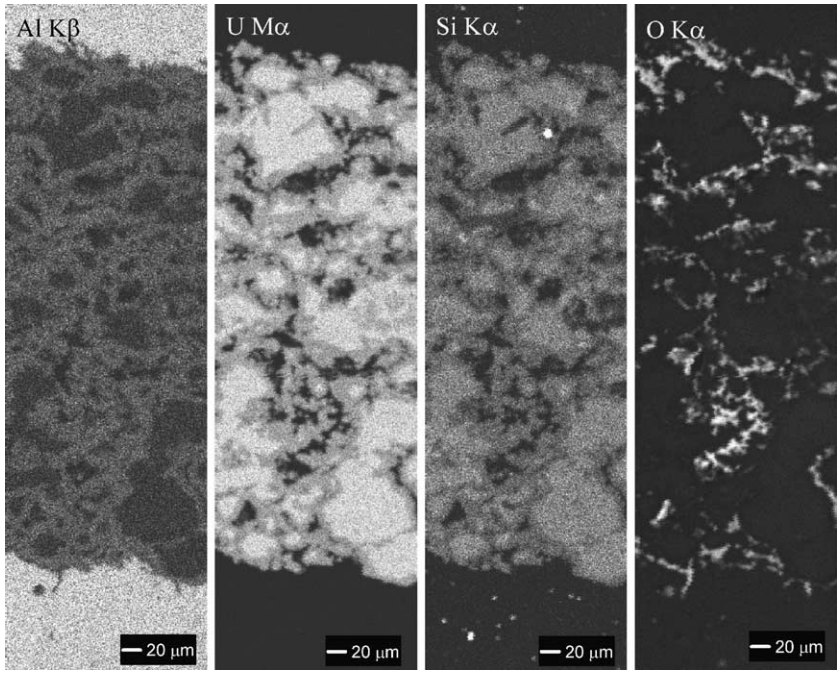

Fig. 5. X-ray maps of, respectively, AlKβ, UMα, SiKα and OKα of an area in the meat of the fuel section that has been submitted to a heat flux of 550 W/cm^2.

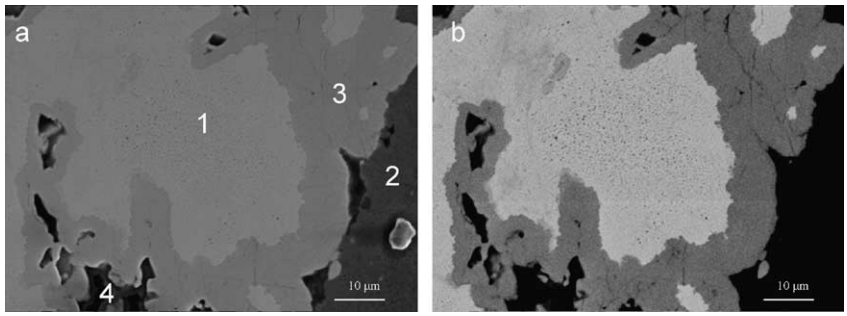

Fig. 6. Secondary electron image (a) of a U_3Si_2 particle (1) at the Al cladding (2). The fuel particle is surrounded by an $U_3Al_7Si_2$ layer (3) and in-between the particles pores have formed (4). The backscattered electron image (b) of the same area reveals several small fission gas bubbles.

Where the fission gases have not yet precipitated in bubbles, the fission product distribution shows a nearly constant concentration in the grain interior. From the X-ray micrographs (Fig. 7) it is seen that the concentration of Xe and Nd is lower in the U–Si–Al mixed phase, but at the interface of this interaction layer with the Al cladding, a clear rise in fission product concentration can be observed, producing a halo of fission products around each fuel grain in the maps. This is reflected in the quantitative linescan data (Fig. 8) where a steep local rise of fission product concentration can be seen at the interface of the interaction layer and the Al cladding (boundary between zones 2 and 3 in Fig. 8). Inside the grain (zone 1), the concentrations are nearly constant, while at the edges of the grain, a shoulder of uranium and fission product concentrations is seen (zone 2) corresponding to the U–Si–Al interaction phase. In between the mixing phase of this grain and the adjacent grain (zone 2) the fission product signals rise again, producing the halo-effect.

The fission product concentrations decrease gradually when approaching the grain edges (limits of zone 1) as a result of the ejection, in contrast to the U concentration that drops suddenly when the edges are reached. Pu, as an activation product, follows the uranium concentration closely. In the cladding, the fission product concentrations are low to non-existent. The range of ejection of the fission products due to their energy after fission (some 10 μm), is clearly visible as a slowly decreasing concentration outside the grains (zone 3).

The fission products Mo and Ru have also been measured but for reason of clarity not added to the

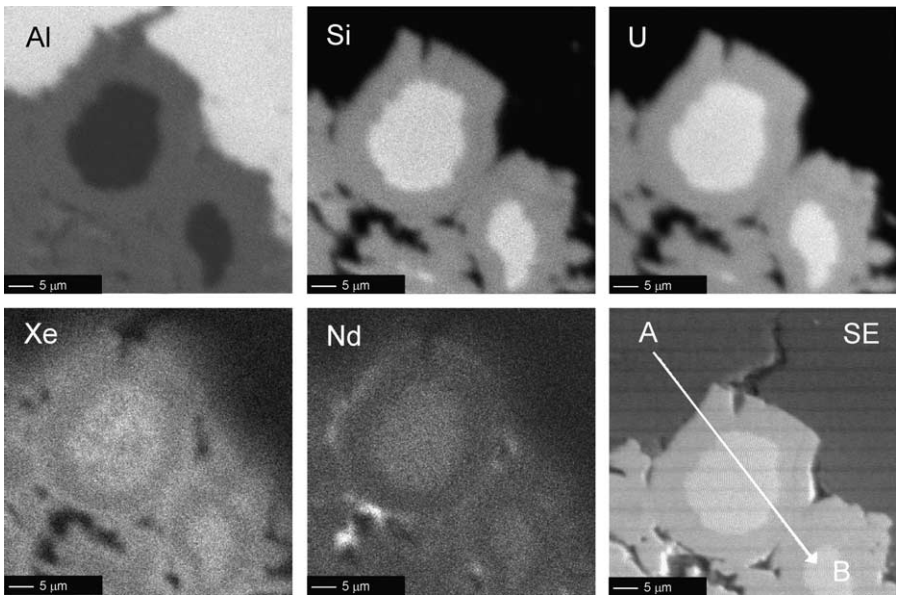

Fig. 7. Local X-ray map (respectively, of AlKβ, UMα, SiKα, XeLα, NdLα) of a U_3Si_2 particle in the Al matrix. The secondary electron image (SE) indicates the position at which a semi-quantitative linescan is measured.

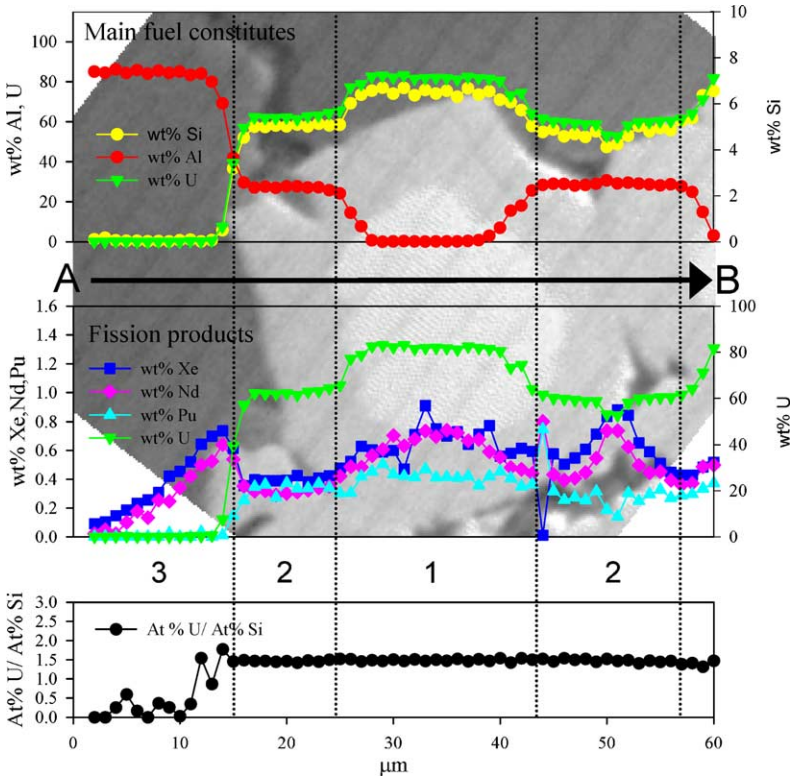

Fig. 8. Semi-quantitative linescan covering the Al matrix and a U_3Si_2 particle defined in Fig. 6. The linescan can be divided in different zones: zone 1 is inside the grain, zone 2 is the interaction layer and zone 3 is the Al matrix.

graph in Fig. 7. Both Mo and Ru show a behavior similar to Xe and Nd. Coalescence and precipitate formation cannot be attained due to too low temperatures. Furthermore, from Fig. 8 it is seen that the ratio of the atomic percentages of U and Si remains constant at around 1.5, even inside the U–Si–Al mixing phase.

4. Discussion

It seems obvious that the failure of the fuel plate is entirely related to the deterioration of the cladding and not to the degradation of the fuel. The microstructural analysis of samples submitted to different heat fluxes, shows the evolution of the fuel plate as the corrosion of the cladding progresses.

Taking into account both the gamma heating and the generated heat flux of 550 W/cm^2, it is estimated that at the spot close to the stiffener, the temperature at the cladding surface of the fuel plate must have reached values between 180 and 200 °C. Although aluminum and aluminum alloys show a good corrosion resistance in aqueous environments through the formation of a protective oxide film, at such high temperatures general corrosion of the Al–Mg alloy will occur. The resulting duplex corrosion layer, consisting of an alumina barrier layer on top of a porous boehmite (γ-AlO(OH)) bulk corrosion layer [7,9], has a much lower thermal conductivity (2.25 W/m K) compared to AG3 NET alloy (130 W/m K) [8]. The increase in temperature of the cladding following the buildup of this duplex layer, will in turn accelerate the corrosion process. The X-ray map in Fig. 4 reveals that in the current case an oxide layer of approximately 100 μm is formed on the cladding surface. With a temperature increase of 1.5–2° per μm of oxide, calculations show that the cladding has reached temperatures in excess of 300 °C (Fig. 9). At these high temperatures, progressing sensitisation of the aluminum–magnesium cladding leads to the decoration of the grain boundaries with Mg_2Al_3 precipitates, making the cladding susceptible to grain boundary corrosion [9,10].

In conjunction with the high cladding temperatures, the meat temperature also rises and the formation of the U–Si–Al interaction zone will speed up, leading to a complete consumption of the pure Al matrix in the fuel. This in turn leads to a deterioration of the thermal conductivity of the meat, which will further increase the temperature. Eventually, as the cladding becomes completely corroded, water will be able to penetrate the fuel matrix as steam and will start to oxidise the meat.

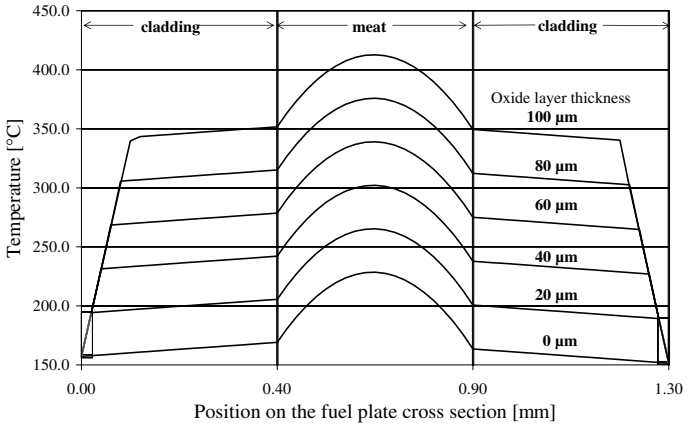

Fig. 9. Results of the thermohydrolic calculations of radial temperature profiles in the hottest zone of the plate. Calculations are performed at a heat flux of approximately 520 W/cm^2 and increasing oxide layer thickness.

Regarding the fuel meat, the behavior of the U_3Si_2 fuel grains seems to have been exemplary. Except for the advanced interaction with the Al of the matrix, they have withstood extreme temperatures for this fuel type, without any deleterious changes in their physical properties. Regular irradiations occur at temperatures below 150–200 °C centerline temperature, while in the current irradiation the fuel was calculated to be exposed to temperatures as high as 220–240 °C. Considering the effect of the 100 μm thick oxide layer, the calculated centerline temperature in fact rises to over 400 °C.

Such extreme temperatures substantiate the observed extent of the interaction layer formed between the U_3Si_2 fuel and the Al matrix [11,12]. Complete consumption of the Al matrix has occurred, an effect that during regular irradiation campaigns has never been witnessed. The composition of the interaction phase is reported to be $U(Al,Si)_3$, which may be in agreement with the currently observed constant U/Si ratio in the interaction phase (Fig. 8). In that case, the formula would be close to $U_3Al_7Si_2$. The position of this compound in the isothermal section of the ternary equilibrium diagram is shown in Fig. 10.

According to the literature, the formation of the interaction phase is expected to lead to some swelling of the elements [4]. Such a phenomenon could not be observed in the current project. The measured swelling of the fuel elements is found to be due to the corrosion of the cladding and not to swelling of the meat.

Concerning fission gas release, the fuel shows a stable behavior with formation of small dispersed fission gas bubbles in the interior of the grains at this stage of the irradiation. There is no evidence of important release of fission gases, which would lead to much lower xenon concentrations in the grains.

The fission product distributions show nearly constant concentrations in the grain interiors, except where

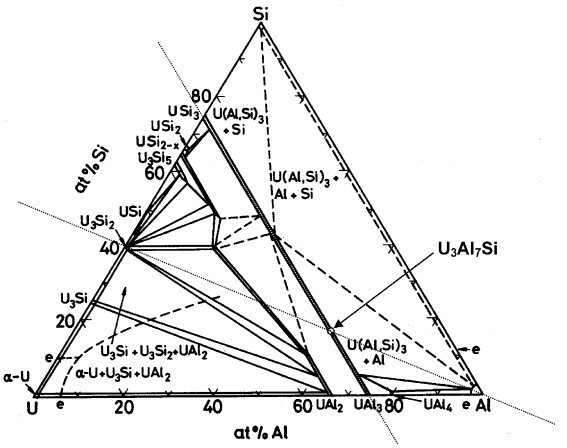

Fig. 10. Isothermal section at 400 °C of the ternary system U–Al–Si [15]. The composition of the interaction layer lies at the intersection of the (dotted) lines U_3Si_2–Al and USi_3–UAl_2.

fission gases have begun to precipitate in bubbles. Fission products that have been ejected out of the grains, have been swept up by the formation of the U–Si–Al interaction phase and have accumulated at the interface between this phase and the remaining aluminum or between two interaction phase fronts of adjacent grains. This produces a halo of higher concentrations around each grain in the X-ray maps.

The origin and development of the observed voids located in the former Al matrix, is not clear. Diffusion phenomena associated with the formation of the interaction phase (the so-called Kirkendall effect [13,14] owing to the diffusion of Al in U_3Si_2) and the accumulation of fission products at the interaction phase fronts are probably responsible for the creation of the voids. Upon water intrusion, considerable oxidation and

lixiviation of the remaining Al matrix and possibly also of the interaction phase could occur. Because the irradiation was stopped shortly after the cladding had failed, the oxidation has remained limited to the surface of the voids, as visible in the X-ray maps showing the oxygen distribution in the meat.

5. Conclusion

The failure of the U_3Si_2 (6.1 g U/cm^3) fuel plate is related to degradation of the cladding, which was submitted to a temperature that exceeds the limit for corrosion resistance of the AG3 NET alloy. The high heat fluxes generated by the fuel have caused cladding temperatures to exceed 180–200 °C, which has caused the creation of thick and porous corrosion layers on the cladding surface. Because of the low thermal conductivity of these layers, temperatures have increased further, which have accelerated the corrosion until the cladding failed and steam was able to reach the fuel.

The fuel itself has retained its integrity without any deleterious changes in the physical properties. The fuel has been exposed to extreme high temperature causing the complete consumption of the matrix by the formation of a $U_3Al_7Si_2$ interaction phase and the creation of voids in the former Al matrix. Upon complete cladding failure, the surfaces of the voids have been oxidised due to the intrusion of steam.

The fission products remain homogeneously dispersed in the fuel grains, except for Xe which has started to form sub-micron intragranular bubbles. The formation of the interaction phase has swept up all fission products that were ejected from the grains, causing an accumulation of fission products at the interface of the interaction layer with the Al matrix and cladding or with the interaction phase front of an adjacent grain.

Acknowledgements

The authors wish to thank G. Cools, D. Delnooz, Y. Parthoens, F. Swinnen and B. Vos for their contributions to this project.

References

[1] G.A. Pon, W.B. Lewis, L.R. Haywood, D.B. Primeau, G.J. Phillips, E.E. Merlo, Report AECL-2010, 1964.
[2] D.B. McCulloch, J.H. Whitfield, Report AAEC/E233, 1972.
[3] S. Nazaré, Mater. Sci. Forum 48&49 (1989) 297.
[4] Safety Evaluation Report NUREG-1313, US Nuclear Regulatory Commission, 1988.
[5] J.L. Snelgrove, G.L. Hofman, M.K. Meyer, C.L. Trybus, T.C. Wiencek, Nucl. Eng. Des. 178 (1997) 119.
[6] J. Marín, J. Lisboa, J. Ureta, L. Olivares, H. Contreras, J.C. Chávez, J. Nucl. Mater. 228 (1996) 61.
[7] K. Wefers, Aluminum 57 (1981) 722.
[8] IAEA-TECDOC 643, vol. 4, 1992.
[9] J.E. Hatch (Ed.), Aluminum: Properties and Physical Metallurgy, American Society for Metals, Ohio, 1984.
[10] K. Videm, J. Nucl. Mater. 2 (1959) 145.
[11] T.C. Wiencek, R.F. Domagala, H.R. Thresh, Nucl. Technol. 71 (1985) 608.
[12] G.L. Hofman, J. Rest, J.L. Snelgrove, T. Wiencek, S. Koster van Goos, in: Proceedings of the International Meeting on Reduced Enrichment for Research and Test Reactors, Seoul, Korea, 1996. Available from <http://www.td.anl.gov/Programs/RERTR/FUELS96/GLHOF296.html>.
[13] K.-H. Kim, J.-M. Park, C.-K. Kim, G.L. Hofman, K.-W. Paik, J. Nucl. Mater. 270 (1999) 315.
[14] S. Nazaré, J. Nucl. Mater. 124 (1984) 14.
[15] H.U. Borgstedt, H. Wedemeyer, in: Gmelin Handbook of Inorganic Chemistry: Uranium Supplement, vol. B2, Springer-Verlag, 1989.